Electron transport in *n*-doped Si/SiGe quantum cascade structures

I. Lazic
School of Electrical Engineering, University of Belgrade, 11000 Belgrade, Serbia and Department of Materials Science and Engineering, Delft University of Technology, 2628 CD Delft, The Netherlands

Z. Ikonic[a)]
School of Electronic and Electrical Engineering, University of Leeds, Leeds, LS2 9JT, United Kingdom

V. Milanovic
School of Electrical Engineering, University of Belgrade, 11000 Belgrade, Serbia

R. W. Kelsall, D. Indjin, and P. Harrison
School of Electronic and Electrical Engineering, University of Leeds, Leeds, LS2 9JT, United Kingdom

(Received 22 December 2006; accepted 28 February 2007; published online 2 May 2007)

An electron transport model in *n*-Si/SiGe quantum cascade or superlattice structures is described. The model uses the electronic structure calculated within the effective-mass complex-energy framework, separately for perpendicular (X_z) and in-plane (X_{xy}) valleys, the degeneracy of which is lifted by strain, and additionally by size quantization. The transport is then described via scattering between quantized states, using a rate equations approach and tight-binding expansion, taking the coupling with two nearest-neighbor periods. Acoustic phonon, optical phonon, alloy disorder, and interface roughness scattering are taken into account. The calculated current/voltage dependence and gain profiles are presented for two simple superlattice structures. © *2007 American Institute of Physics*. [DOI: 10.1063/1.2722244]

I. INTRODUCTION

Following the successful realization of GaAs/AlGaAs-based terahertz quantum cascade lasers,[1] Si/SiGe quantum cascade structures are attracting considerable attention as a very promising technology for the same purpose. This would offer compatibility and even the possibility of monolithic integration with the standard complementary metal-oxide semiconductor (CMOS) technology. Within the Si/SiGe system, the *p*-doped structures have been explored in much more detail, because of larger discontinuity of the valence band at heterointerfaces, which makes them applicable not only in terahertz, but also in midinfrared range. For terahertz emission, however, even modest discontinuities may suffice, which makes *n*-doped structures also interesting, and here we report on modeling the electron transport and light gain/absorption in *n*-Si/SiGe cascades. We have previously performed extensive modeling of hole transport,[2] demonstrated the growth of *p*-Si/SiGe strain-symmetrized cascades with up to 1200 layers, and observed terahertz electroluminescence from them.[3] Midinfrared luminescence has been observed by another group.[4] In this article we consider electron transport and the possibility of achieving gain in *n*-doped Si/SiGe cascade structures. There are numerous differences compared to the transport in *n*-doped GaAs/AlGaAs cascades, both because one of the major scattering processes—polar LO-phonon scattering—does not exist in Si/SiGe, and because of the presence of two types of quantized electronic states and degeneracies in this system.

A previous study of *n*-Si/SiGe quantum cascade structures[5] has considered the operation of a triple quantum well active region within the unity injection approximation, accounting for a limited number of scattering processes and of states present in this system, using a combined (scattering and tunneling) approximate description of transport. In this work we present a fully consistent model of scattering-induced transport in *n*-Si/SiGe cascades, accounting for different types of quantized states and relaxation processes coupling them, and apply it to two simple superlatticelike structures.

II. THEORY AND COMPUTATIONAL DETAILS

In pure Si and in $Si_{1-x}Ge_x$ alloys with $x<0.85$, the conduction band minima occur near the X point of the Brillouin zone, and the low-lying conduction band quantized states in a Si/SiGe multilayer structures hence originate from the six X valleys. The X valleys are anisotropic, having different longitudinal and transverse effective mass. To find the electronic subband structure, we employ the effective mass envelope function Schrödinger equation. For structures grown on the conventional [001] oriented substrate, the two X valleys with their axes parallel to the growth direction (denoted as X_z) give rise to quantized subbands different from those of four X valleys whose axes are perpendicular to the growth direction (denoted as X_{xy}). This is because the quantization effective masses are different in the two cases, amounting to $m_l=0.916m_e$ and $m_t=0.19m_e$ in both materials, where m_e is the free-electron mass. Furthermore, the different lattice constants of Si and Ge imply that layers in Si/SiGe structure are uniaxially strained, the amount of strain being set by the choice of the substrate composition (Ge molar fraction x_s), in turn chosen so as to achieve strain balance. The in-plane

[a)]Electronic mail: z.ikonic@leeds.ac.uk

lattice constant of the epilayer material equals that of the substrate, while the perpendicular lattice constant changes. The strain lifts the degeneracy between the six X valleys, and hence also influences the subband energies. The potential energy (position of the X valley bottom) in a strained $Si_{1-x}Ge_x$ alloy layer, measured from the valence band top of the substrate, is calculated accounting for the uniaxial and hydrostatic strain induced shifts, according to[6]

$$E_{\mathrm{cond}}^{X} = -\frac{\Delta_{\mathrm{so}}(x_s)}{3} + \Delta E_{v,\mathrm{av}}(x,x_s) - \Delta E_{v,\mathrm{av,hyd}}(x,x_s) + \frac{\Delta_{\mathrm{so}}(x)}{3} + E_g(x) + \Delta E_{\mathrm{hyd}}^{H}(x,x_s) + \Delta E_{\mathrm{uni}}^{X}(x,x_s), \quad (1)$$

where X stands for either X_z or X_{xy}, Δ_{so} is the composition dependent spin-orbit splitting, $\Delta E_{v,\mathrm{av}}=(x-x_s)(0.74-0.06x_s)$ (eV) is the average valence band offset between relaxed substrate and this alloy, $E_g(x)=1.17-0.34x+0.206x^2$, is the (experimental) band gap of the alloy, $\Delta E_{v,\mathrm{av,hyd}}=a_V(2\varepsilon_{xx}+\varepsilon_{zz})$ is the hydrostatic strain component induced change of the valence band offset, $\Delta E_{\mathrm{hyd}}^{H}=(\Xi_d+\Xi_u/3)(2\varepsilon_{xx}+\varepsilon_{zz})$ the hydrostatic strain component induced shift of the X valley edge, while $\Delta E_{\mathrm{uni}}^{X_z}=2\Xi_u(\varepsilon_{zz}-\varepsilon_{xx})/3$ and $\Delta E_{\mathrm{uni}}^{X_{xy}}=-\Xi_u(\varepsilon_{zz}-\varepsilon_{xx})/3$ are the uniaxial strain component induced shifts of the X valley edge (different for the two types of X valleys). The strain components in a layer are given by $\varepsilon_{xx}=\varepsilon_{yy}=a/a_0-1$ and $\varepsilon_{zz}=-(2C_{12}/C_{11})\varepsilon_{xx}$, where a_0 and a are lattice constants of unstrained layer and substrate, respectively. The lattice constant of an unstrained layer with Ge mole fraction x is given by $a(x)=a_{\mathrm{Ge}}x+a_{\mathrm{Si}}(1-x)+b_{\mathrm{bow}}x(1-x)$.

The material constants used in this calculation are $a_V=-4.54(-3.1)$, for Si (Ge) and linear interpolation for the $Si_{1-x}Ge_x$ alloys, $\Xi_u=8.6$ (9.4) and $\Xi_d=-6.0$ (−4.92), $C_{11}=1.675$ (1.315), $C_{12}=0.650$ (0.494), $a=0.543(0.565)$ nm for Si (Ge). Linear interpolation is used for the $Si_{1-x}Ge_x$ alloy parameters, except for the lattice constant where bowing was taken into account, with $b_{\mathrm{bow}}=0.001\ 88$ nm.

For practically realizable, strain balanced structures, with Si and SiGe layers grown on a substrate with composition in between, the Si layers are found to be quantum wells for both types of electrons (valleys), with X_z valley shifted below and X_{xy} valley above their position in unstrained Si, and the opposite holds for SiGe alloy layers, implying much shallower wells for X_{xy} than for X_z electrons. Combined with the fact that m_l is over 4 times larger than m_t, the lowest couple of subbands will stem from the X_z valley, and these are much more strongly bound than X_{xy} valley subbands.

The spectrum of quantized states in Si/SiGe quantum wells is somewhat more complicated than suggested by the above effective-mass model, because the two degenerate X_{+z} and X_{-z} valleys are coupled by the potential discontinuity at the heterointerfaces; hence, their equivalent quantized states will in fact mix and split in energy. The wave functions of these states are approximately equal to an even or an odd linear combination of the effective-mass wave functions. The split states can be found within a microscopic framework such as the tight binding[7] or the pseudopotential[8] method (and the coupling constant found in this manner may then be reimported into the effective-mass picture). However, these calculations show that for well widths of interest in this work the intervalley interference induced splitting is rather modest (typically a few meV),[7] and is further decreased if interdiffusion at the interface is accounted for,[8] which enables the translation of state splitting (and consequently the presence of slightly different transition energies) into an increased linewidth of intersubband transitions, and the use of the effective-mass method as a good approximation. This is the approach followed in the present work, and the states derived from the X_z valleys are then twofold, and those from the X_{xy} valleys fourfold degenerate.

In biased quantum cascade structures the subbands are not strictly discrete, since resonances exist in the continuum, but in most cases, e.g., in conventional III-V based cascades, these are sufficiently sharp that essentially the same results may be obtained by solving the Schrödinger equation for discrete states (with real energies), using box boundary conditions. The shallow wells present for X_{xy} electrons in Si/SiGe would make such an approach inappropriate. Therefore, we have used the complex energy method,[9] as has occasionally been applied to quantum cascade structures before.[10] The subband (resonance) energies are allowed to take complex values, with the imaginary part representing the tunneling rate. While virtually no difference is observed in the results for well-bound states, in the case of weakly bound states the wave functions corresponding to these resonances are better "discrete representatives" of the continuous spectrum than the wave functions obtained with real-energy box boundary conditions, and can thus be reliably used in scattering rate calculations. In addition to the more complex procedure required for finding the complex resonant states, there arises an ambiguity in the way in which the complex energies are used in the calculation of scattering rates, which requires real energies. While there is no general recipe for such situations, in the structures considered the imaginary part of the energy was much smaller than the real part; hence, only the latter was used in further calculations.

The calculation of electron transport in a cascade, described below, requires all states to be assigned to individual periods of the structure. Among all the states found in a finite multiple period structure, for which the resonant states are actually calculated, some are assigned to belong to the reference ("central") period based on their localization properties, and then are replicated (shifted in space and energy) to obtain states assigned to the neighboring periods.

Electrons in the structure change their quantum states by scattering with phonons, on interface roughness, alloy disorder, ionized impurities, and by carrier-carrier scattering. In this article we consider the first three mechanisms, and take small enough doping that the last two can be neglected. Furthermore, we take that photon emission/absorption processes do not contribute significantly to the electron transport (cascade operation below lasing threshold). With two equivalent X_z and four equivalent X_{xy} valleys, there are just as many sets of degenerate subbands. Some scattering processes cause the electrons to change the valley they belong to (and perhaps also the subband index), and others only act within different subbands of the same valley.

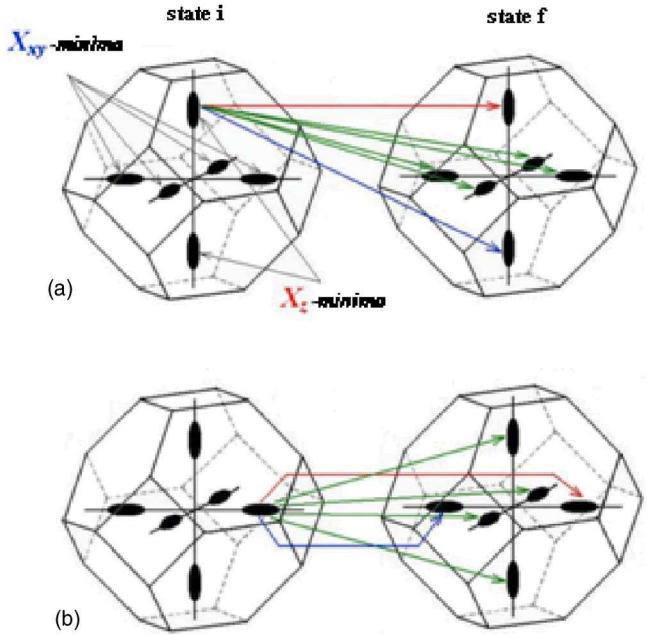

FIG. 1. (Color online) Scattering processes in *n*-Si/SiGe structures, for the initial state in (A) X_z, and (b) X_{xy} valley: between subbands of the same valley (red), *f*-processes (green), and *g*-processes (blue).

If the initial and final states belong to different *X* valleys, the (intervalley) scattering is caused by large wave vector phonons. Processes in which an electron scatters between two *X* valleys oriented at 90°, e.g., X_{+z} and X_{+y}, are *f*-processes, and those between two valleys oriented at 180°, e.g., X_{+z} and X_{-z}, are *g*-processes. It should be noted, therefore, that two X_z valley subbands can be coupled by *g*-processes (e.g., if the initial state belongs to X_{+z}, and the final to X_{-z}). Some of these processes are "allowed" and others are "forbidden." On the other hand, small wave vector acoustic phonons only cause transitions between states belonging to the same valley, e.g., both to X_{+z}, and the same is assumed for interface roughness and alloy disorder scattering, while small wave vector optical phonons do not induce intravalley scattering at all. Various scattering processes in this system are illustrated in Fig. 1. The phonon scattering rates are calculated according to Ref. 11 and the last two scattering rates according to Ref. 12. The energy-dependent scattering rates are then averaged over the in-plane electron distribution, allowing the electron temperature to differ from the lattice temperature. In numerical calculations we use the parameter values for Si as a good approximation, because this is the well material where most of the wave functions are localized. The phonon scattering parameters were taken from Ref. 13 and for the interface roughness scattering we used the values $\Delta=0.4$ nm and $\Lambda=16$ nm (as indicated by TEM images of *p*-doped Si/SiGe samples used in our previous work[3,14]).

When tracking the electron distribution over quantized states, set by all the scattering processes involved, one has two choices in this system which has degenerate, or almost degenerate, states. One choice is to track the population of each single state, and the other to consider only the population of the full group of degenerate states, knowing that the electron population is shared evenly between the members of the degenerate set because there is no mechanism which would dictate otherwise. We use the second choice because it considerably reduces the total number of states to handle explicitly. It should be noted, however, that one then needs more care in finding the total scattering rate between two states, being mindful of their degeneracy. For example, the scattering-induced transition which, within this "grouped states" description, is denoted as $X_z^i \rightarrow X_z^f$, where the superscript labels the quantized state, consists in fact of the following transitions between individual states: $X_{+z}^i \rightarrow X_{+z}^f$ (caused by acoustic phonons, alloy and interface scattering), and $X_{+z}^i \rightarrow X_{-z}^f$ (caused by *g*-processes), or of the analogous two transitions starting with the "$-z$" initial state. As another example, the transition $X_z^i \rightarrow X_{xy}^f$ is composed of $X_{+z}^i \rightarrow X_{+x}^f$, $X_{+z}^i \rightarrow X_{-x}^f$, $X_{+z}^i \rightarrow X_{+y}^f$, and $X_{+z}^i \rightarrow X_{-y}^f$, all of which are caused by *f*-processes, and are equal among themselves, so only one of the rates has to be evaluated, and then simply multiplied by 4 to be used in any further calculation.

We denote with n_i the electron concentration in the quantum state *i* of the "central" period, and explicitly account for *N* such relevant states (some of them being of X_z, others of X_{xy} type). We assume periodicity of the electron distribution, i.e., $\ldots=n_{i-N}=n_i=n_{i+N}=n_{i+2N}=\ldots$ for every $i=1,2,\ldots,N$, where $i+N$ and $i+2N$ denote the *i*th state of the first and second period to the right of the "central" one, respectively, and, correspondingly, we assume charge neutrality of each period, i.e., $\Sigma_{i=1}^N n_i=N_D$, where N_D is the donor doping density per period. Using the shift-invariance of scattering rates $w_{i\rightarrow f}$, evaluated as described above, the system of rate equations reads

$$\frac{dn_i}{dt} = -n_i \sum_{j=1}^{N} (w_{i\rightarrow j} + w_{i\rightarrow j+N} + w_{i+N\rightarrow j} + w_{i\rightarrow j+2N} + w_{i+2N\rightarrow j}) + \sum_{j=1}^{N} (w_{j\rightarrow i} + w_{j\rightarrow i+N} + w_{j+N\rightarrow i} + w_{j\rightarrow i+2N} + w_{j+2N\rightarrow i}) n_j. \quad (2)$$

In the steady state one of the equations is replaced by the charge neutrality condition. One could add the thermal balance rate equations to find electron distribution of each subband. In the present calculation, however, we did not use such an elaborate model, and electron temperatures were set to fixed values, larger than the lattice temperature and chosen to lie within the range found in previous calculations in *p*-Si/SiGe cascades.[2]

After finding the electron distribution over the subbands of the X_z and X_{xy} valleys, the absorption (or gain) profile can be calculated. Within the effective mass model, intersubband optical transitions are allowed only between quantized states derived from the same valley, e.g., both from X_{+z}, or both from X_{-z}, etc. Within the more accurate split-states picture, out of the four possible transitions between the initial quantized state doublet and the final state doublet, only two are allowed and their matrix elements are very close to those obtained within the effective mass model.[8] These selection rules imply that the equivalent-valley (quasi)degeneracy in Si/SiGe has the same effect as the spin degeneracy of Γ valley subbands in conventional III/V based structures, with

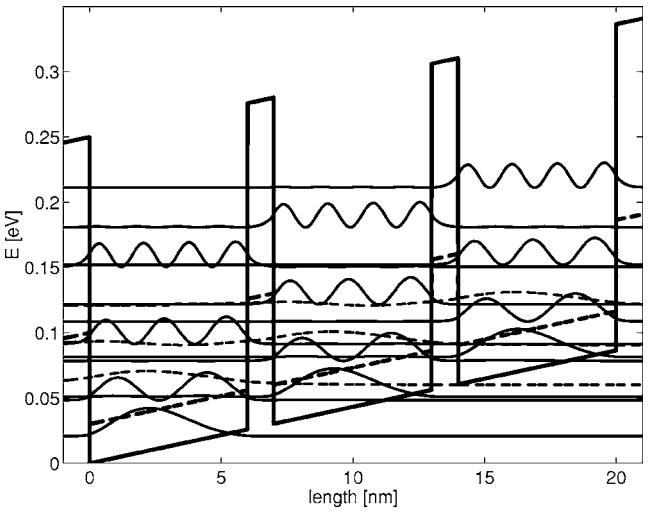

FIG. 2. An example of the subbands calculated in the structure (A). The X_z and X_{xy} valley edges are shown by solid and dashed lines, respectively, and the state energies are given by the corresponding wave function base lines. Note that the wave functions of the four lowest X_z states (solid) are rather strongly localized, but the lowest X_{xy} state (dashed) is quite leaky.

the spin-conservation selection rule holding in optical transitions (the spin degeneracy is present in this system as well). Therefore, the conventional expressions for optical absorption/gain in Γ valley intersubband transitions are directly applicable here. In a quantum cascade structure both the "intraperiod" and "interperiod" intersuband optical transitions contribute, and the calculation is performed according to the expression given in Ref. 15.

III. RESULTS AND DISCUSSION

Numerical calculations were performed for two very simple cascade structures (essentially superlattices, rather than complex-period cascades normally employed for intersubband lasers), having a single well and barrier per period. The structures are: (A) Si (6 nm)/$Si_{0.65}Ge_{0.35}$ (1 nm), and (B) Si (8 nm)/$Si_{0.6}Ge_{0.4}$(1 nm), and both are assumed grown on a $Si_{0.95}Ge_{0.05}$ substrate for strain balance. The X_z state spacing is in the tens of meV range (precise values depending on the bias, but approximately 27 and 20 meV between the lowest two states, respectively), and there is just one X_{xy} state that is significantly localized in the wells, lying between the first and second excited X_z states. Due to the narrower wells, the wave functions in structure (A) are more leaky than in (B). An example of the subbands calculated in structure (A) is given in Fig. 2. The wave functions of the four lowest X_z states are quite strongly localized in single wells, but the lowest X_{xy} state wave function extends well into the next period.

In the electron transport calculation in these structures, the donor doping was assumed to be 10^{11} cm^{-2} per period, the lattice temperature was set to 20 K, and the carrier temperatures to 150 K (A) and 100 K (B). The calculated population of states and the current, as they depend on the bias, are shown in Figs. 3 and 4. The populations vary very nonmonotonously over the wide range of bias fields displayed, as one or the other scattering process becomes dominant. The current peaks generally correspond to values of bias where

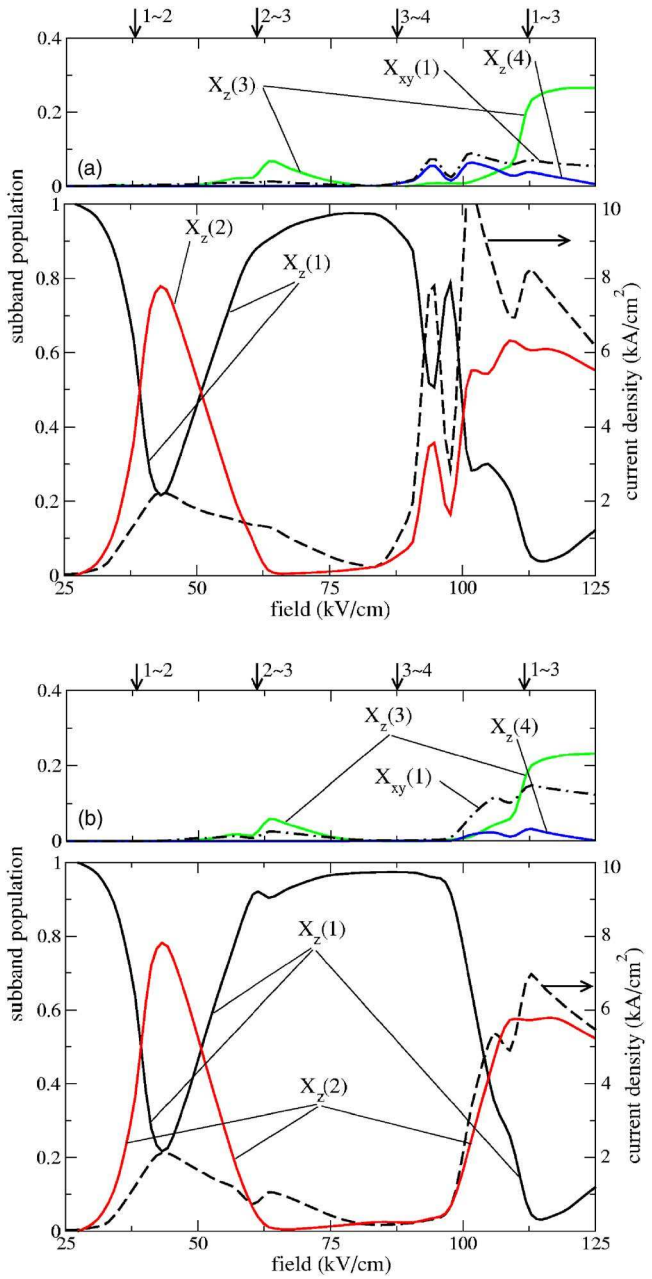

FIG. 3. (Color online) The population of X_z subbands (solid lines) and the X_{xy} subband (dot-dashed line), and the current density (dashed line) calculated for Si/SiGe superlattice structure (A) described in the text, using two nearest-neighbor (a) and only the first-nearest-neighbor (b) coupling. The lower pane shows the lowest two X_z subbands, and population of other subbands is shown in the upper pane, for clarity. The arrows on top, annotated as $m \sim n$, show the values of bias where state m of one period anticrosses with the state n from the next lower period.

anticrossing (alignment) of states in subsequent periods appears, which indicates the importance of quasielastic scattering processes. It is interesting to note, by comparing Fig. 3(a) and 3(b), that including the second-nearest-neighbor coupling is significant only for high bias fields in the more "leaky" structure (A), while there are almost no differences for the structure (B).

Of importance for the possibility of achieving gain, there clearly exist ranges of bias fields in both structures where an inversion appears between two subsequent X_z states (i.e., where the transition matrix element can be significant). In

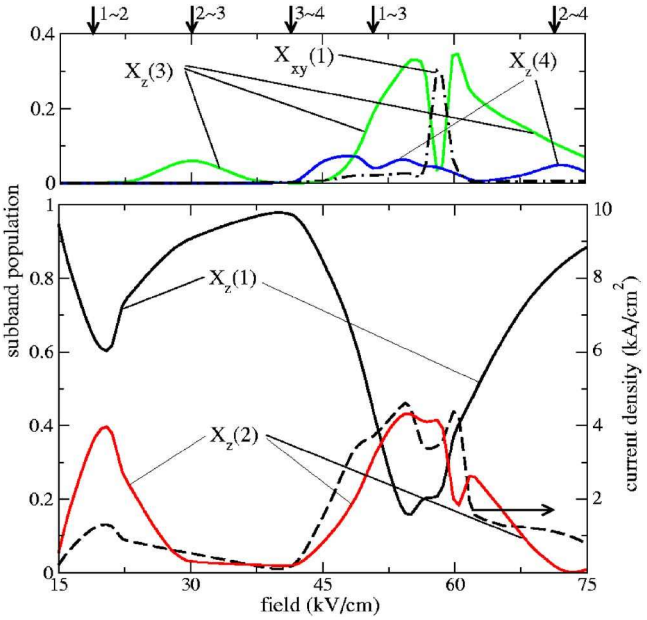

FIG. 4. (Color online) Same as in Fig. 3, but for the structure (B). The results obtained with one- or two-nearest-neighbor coupling are almost identical here.

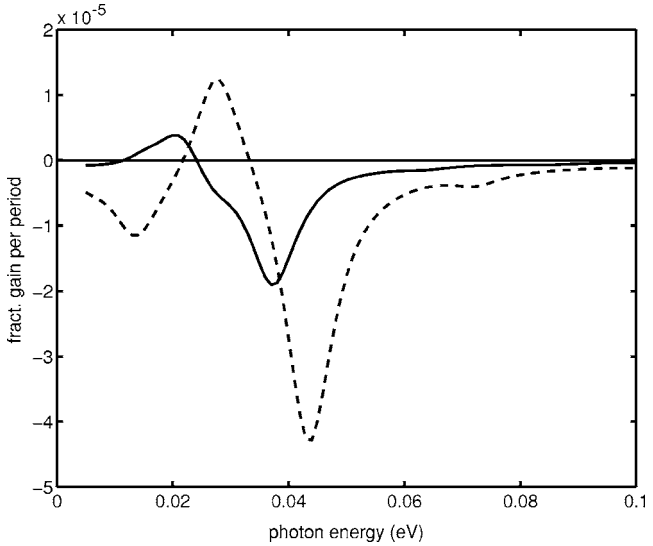

FIG. 5. The fractional (per period) gain/absorption profile calculated for the superlattice (a) biased at 43 kV/cm (dashed line), and superlattice (b) biased at 56 kV/cm (solid line). The luminescence line FWHM was set to 10 meV, and electron surface density to 10^{11} cm^{-2} per period.

particular, the more leaky structure (A) is predicted to offer a peak inversion of 54% between the lowest two $X_z$states, X_z^2 and X_z^1 in the same well, around the anticrossing of the ground state in one and the first excited state in the nearest lower period, at about 43 kV/cm bias. The inversion does not appear at the corresponding bias in the less leaky structure (B), because the electron transfer rate between the wells is slower and the electrons have more time to relax to the ground state. However, an inversion of 22% between X_z^2 and X_z^1 states appears at a larger bias (54 kV/cm) in structure (B), this time with the aid of other states which also have significant populations in this bias range.

For the gain to be sustainable and useful, however, the operating point of the structure should not be in the range where the differential resistance is negative, otherwise domain formation is likely to occur, which would drive the device away from the desired operating point. A closer look at Figs. 3 and 4 shows that there are, albeit narrow, ranges of bias where population inversion coexists with stable operating points.

The calculated fractional gain/absorption profiles for the two structures, biased at suitably chosen fields, are shown in Fig. 5, where a linewidth (FWHM) of 10 meV was assumed. Interestingly, despite the different well widths both structures have almost the same value of dipole matrix element for the $X_z^2 \rightarrow X_z^1$ transition, amounting to 1.3 nm, apparently due to the comparatively more widespread (leaky) wave functions in the narrow-well structure (A). By dividing the fractional gain by the length of the period, a peak gain coefficients of 18.6 cm^{-1} (at photon energy of 27 meV) is obtained for structure (A), and 4.4 cm^{-1} (at 21 meV) for structure (B), the former being in the range of practical interest. The gain scales linearly with the doping density, but additional scattering mechanisms which were here neglected (carrier-carrier and ionized impurity scattering) would have to be included in calculation for large values of doping. Certainly, further improvements may be expected from a more complex cascade design.

IV. CONCLUSION

We have considered electron transport in *n*-Si/SiGe cascade or superlattice structures, using the rate equations approach and tight-binding expansion, taking the coupling with two nearest-neighbor periods. Acoustic phonon, optical phonon, alloy and interface roughness scattering are taken in the model. The calculated current/voltage dependence and gain profiles are presented for two simple superlattice structures. The existence of significant gain is predicted, occurring at operating points with positive differential resistance, although in narrow ranges of bias fields. In the examples investigated in this work, most of the electrons populate the X_z states, while the population of the X_{xy} states becomes significant only at very high bias fields, implying that the existence of the latter can usually be neglected. However, by manipulating the strain conditions situations may be created in which the X_{xy} state(s) might behave as the principal current carrying states, which would feed appropriate X_z states with electrons, in order to achieve population inversion.

ACKNOWLEDGMENT

The authors are grateful to the Royal Society (U.K.) for support.

[1] R. Kohler, A. Tredicucci, F. Beltram, H. E. Beere, E. H. Linfield, A. G. Davies, D. A. Ritchie, R. C. Iotti, and F. Rossi, Nature **417**, 156 (2002).
[2] Z. Ikonic, P. Harrison, and R. W. Kelsall, J. Appl. Phys. **96**, 6803 (2004).
[3] R. Bates, S. A. Lynch, D. J. Paul, Z. Ikonic, R. W. Kelsall, P. Harrison, S. L. Liew, D. J. Norris, A. G. Cullis, W. R. Tribe, and D. D. Arnone, Appl. Phys. Lett. **83**, 4092 (2003).
[4] G. Dehlinger, L. Diehl, U. Gennser, H. Sigg, J. Faist, K. Ensslin, D. Grutzmacher, and E. Muller, Science **290**, 2277 (2000).
[5] S. Ghosh, B. Mukhopadhyay, and P. K. Basu, Microwave Opt. Technol. Lett. **35**, 470 (2002).

[6]G. Curatola and G. Iannaccone, Nanotechnology **13**, 267 (2002).
[7]T. B. Boykin, G. Klimeck, M. A. Eriksson, M. Friesen, S. M. Coppersmith, P. V. Allmen, F. Oyafuso, and S. Lee, Appl. Phys. Lett. **84**, 115 (2004).
[8]A. Valavanis, Z. Ikonic, and R. W. Kelsall (unpublished).
[9]M. Wagner and H. Mizuta, Phys. Rev. B **48**, 14393 (1993).
[10]C. Y. L. Cheung, P. Rees, K. A. Shore, and I. Pierce, J. Mod. Opt. **47**, 1857 (2000).
[11]F. Monsef, P. Dollfus, S. Galdin, and A. Bournel, Phys. Rev. B **65**, 212304 (2002); F. Monsef, P. Dollfus, S. Galdin, and A. Bournel, Phys. Rev. B **67**, 059903 (2003).
[12]T. Unuma, M. Yoshita, T. Noda, H. Sakaki, and H. Akiyama, J. Appl. Phys. **93**, 1586 (2003).
[13]P. Dollfus, J. Appl. Phys. **82**, 3911 (1997).
[14]A. G. Cullis and M. Califano (private communication).
[15]V. D. Jovanović, S. Hofling, D. Indjin, N. Vukmirovic, Z. Ikonic, P. Harrison, J. P. Reithmaier, and A. Forschel, J. Appl. Phys. **99**, 103106 (2006).